5658 *Biochemistry* **2009,** *48,* 5658–5668
DOI: 10.1021/bi900402c

BIOCHEMISTRY
including biophysical chemistry & molecular biology
Article

Molecular Imaging of Lipid Peroxyl Radicals in Living Cells with a BODIPY−α-Tocopherol Adduct[†]

Armen Khatchadourian,[‡] Katerina Krumova,[§] Sebastien Boridy,[‡] An Thien Ngo,[§] Dusica Maysinger,*[,‡] and Gonzalo Cosa*[,§]

[‡]*Department of Pharmacology and Therapeutics, McGill University, 3655 Promenade Sir William Osler, Montreal, Quebec, Canada H3G 1Y6, and* [§]*Department of Chemistry, McGill University, 801 Sherbrooke Street West, Montreal, Quebec, Canada H3A 2K6*

Received March 9, 2009

ABSTRACT: An increasing number of reports discuss the role reactive oxygen species (ROS) have in cellular pathologies and cellular signaling processes. Critical to elucidating the underlying chemical mechanism behind these biological processes is the development of novel sensors and reporters with chemical sensitivity and, more importantly, molecular specificity, enabling the spatial and temporal monitoring of a specific ROS concentration in live cells. Here we report for the first time on the application of BODIPY−α-Tocopherol adduct (B−TOH), a novel lipophilic fluorescent antioxidant indicator, toward detection of peroxyl radicals in model lipid membranes and their imaging in the lipid membrane of live cells. Studies conducted in model lipid membranes show a 5-fold fluorescence enhancement upon reaction of liposome-embedded B−TOH with peroxyl radicals. The enhancement is independent of the solution pH and membrane composition. In studies in live cells performed under states of growth factor withdrawal and increased oxidative stress, a significant increase in B−TOH emission was also observed. Exogenous sources of free radicals were utilized herein, namely, *N*,*N*′-dimethyl-4,4′-bipyridinium dichloride (also known as methyl viologen or paraquat) and uncoated nonemissive CdTe nanoparticles, a source of Cd^{2+}. The recorded fluorescence intensity of B−TOH was proportional to the concentration of the dye and to the level of cellular oxidative stress. By employing fluorescent dyes such as Lysotracker and Nile Red, we demonstrate the formation of peroxyl radicals in subcellular locations in rat pheochromocytoma (PC12 cells) and in primary mouse hippocampal neural cells under oxidative stress conditions. Specifically, we observed peroxyl radicals in lysosomes. The assessment of the subcellular distribution of B−TOH in living cells deprived from growth factors and/or under oxidative stress may be useful in the future in determining subcellular sites of lipid peroxidation. In summary, results from this study underscore the potential of B−TOH as a sensitive and specific probe enabling the molecular imaging of peroxyl radicals in the lipid membranes of live cells.

Reactive oxygen species (ROS)[1] such as peroxyl radicals, hydrogen peroxide, or superoxide radical anion have long been implicated in oxidative damage inflicted on fatty acids, DNA, and proteins as well as other cellular components (*1*). Mounting evidence suggests that ROS act as messengers in cellular signaling, a new paradigm in the rich and diverse chemistry of ROS which has attracted a growing level of attention in the past decade (*1*−*4*).

A significant body of work, both in model membrane systems and in live cells, has examined the role lipid peroxyl radicals play in damaging the cell lipid milieu. Autoxidation of polyunsaturated fatty acid residues is initiated by a free radical such as the hydroxyl radical, which upon reaction with fatty acids generates lipid carbon-centered radicals (eq 1, Scheme 1) (*5*−*7*). Lipid carbon-centered radicals in turn readily trap molecular oxygen under physiological conditions to form lipid peroxyl radicals (*8*, *9*), effective chain carriers in the lipid chain autoxidation (eqs 2 and 3, Scheme 1). In the oxidation process, fatty acyl chains mostly in their *cis* configuration are either converted to the *trans* configuration (*7*, *10*) or form corresponding hydroperoxides and alcohols (*7*, *11*) or may fragment into electrophilic α*β*-unsaturated aldehydes (*11*, *12*), among others. Peroxidation and destruction of the *cis* double bonds may in turn lead to a reduction in the membrane fluidity (*13*) and the appearance of liquid-ordered domains (*14*). Autoxidation of polyunsaturated fatty

[†]A.K. acknowledges the support of a McGill Graduate Studies Fellowship. S.B. is supported by a Doctoral Research Award from CIHR and is a recipient of Max Stern Fellowship award, awarded by the Max Stern Foundation. A.T.N. and K.K. thank the McGill Chemical Biology Fellowship Program (CIHR) for postgraduate scholarships. The studies were supported by grants from CIHR (D.M.), NSERC and CFI (D.M. and G.C.), ADUSA (D.M.), and FQRNT (G.C.).

*To whom correspondence should be addressed. E-mail: dusica.maysinger@mcgill.ca and gonzalo.cosa@mcgill.ca.

[1]Abbreviations: ROS, reactive oxygen species; PC12, rat pheochromocytoma; PS, phosphatidylserine; B−TOH, BODIPY−α-tocopherol adduct; TOH, α-tocopherol; PeT, photoinduced electron transfer; DMPC, dimyristoylphosphatidylcholine; EggPC, egg phosphatidylcholine; ABAP, 2,2′-azobis(2-methylpropionamidine) dihydrochloride; PBS, phosphate-buffered saline; CdTe np, CdTe nanoparticle; NAC, *N*-acetylcysteine; DLPC, dilinoleoylphosphatidylcholine; POPC, palmitolyloleoylphosphatidylcholine; SH-SY5Y, neuroblastoma; HNE, 4-hydroxy-2-nonenal; DOPC, dioleoylphosphatidylcholine; MPA, mercaptopropionic acid.

 Published on Web 04/10/2009

acid residues ultimately generates a variety of secondary cytotoxic products which account for pathological effects, e.g., neurodegenerative diseases (*15*), atherosclerosis (*16*), and cell apoptosis (*17*).

In recent years, it has become apparent that chemical reactions between peroxyl radicals and lipids may in addition play a critical role in cellular signaling (*3*, *4*, *18*). Oxidative signaling pathways arise from the formation of electrophilic α*β*-unsaturated aldehydes which may undergo reaction with nucleotides (indirect signaling) (*4*). Additional oxidative signaling pathways have been reported which involve cardiolipin peroxidation and release of proapoptotic factors from mitochondria (*19*), as well as phosphatidylserine (PS) oxidation in the plasma membrane leading to externalization and recognition of PS on the cell surface by phagocytes (*20*).

Critical to elucidating the underlying chemical mechanism behind cellular pathologies and cellular signaling process is the development of novel probes with the partition, chemical sensitivity, and molecular specificity enabling the spatial and temporal imaging of peroxyl radicals in the lipid membranes of live cells. We have recently made significant progress in this direction by preparing a lipid soluble probe capable of reporting the presence of peroxyl radicals in homogeneous solution. The two-segment receptor−reporter-type free radical scavenger fluorophore probe B−TOH [a BODIPY−α-tocopherol adduct (Scheme 1)] satisfies the necessary specificity, sensitivity and spectroscopy requirements (*23*, *24*).

The molecular specificity of B−TOH arises from the potent lipid peroxyl radical scavenging activity conferred by the chromanol ring in the receptor segment. This chromanol ring architecture mirrors that found in α-tocopherol, the most active naturally occurring lipid soluble antioxidant (*25*) (see eqs 4 and 5 in Scheme 1 for rate constant values for radical scavenging by α-tocopherol). We have shown that B−TOH is nearly as reactive as α-tocopherol in the reaction involving H-atom transfer to a peroxyl radical (eq 4 in Scheme 1). The rate constant for H atom transfer measured for B−TOH in toluene (k_{inh} = 1.0 × 10^6 M^{-1} s^{-1}) is only 0.63-fold that of 2,2,5,7,8-pentamethyl-6-hydroxychroman (k_{inh} = 1.6 × 10^6 M^{-1} s^{-1}), an α-tocopherol analogue lacking the phytyl tail (*23*).

B−TOH sensitivity is given by an intramolecular photoinduced electron transfer (PeT) "off−on" switch activated following reaction with peroxyl radicals (*23*, *26*). Fast intramolecular PeT from the receptor segment (chromanol ring) to the reporter segment (BODIPY dye) renders the probe nonemissive. Upon peroxyl radical scavenging, oxidation of the receptor segment deactivates PeT, leading to a 10-fold fluorescence enhancement.

Here we report for the first time results on the detection of peroxyl radicals in model lipid membranes and real-time imaging of peroxyl radicals in the lipid membranes of live cells, studies which were conducted with B−TOH.

To explore the role of membrane composition and pH in the activity and sensitivity of B−TOH, we initially characterized the fluorescent properties of B−TOH in liposomes (water-filled unilamellar lipid bilayers). This was a necessary preliminary step to our studies within the complex environment of the cell milieu. We next performed experiments with live cells. Our ultimate objective was to assess the suitability of B−TOH for detection of peroxyl radicals in the lipid membrane of living cells in two different models: rat pheochromocytoma (PC12 cells) and mouse primary hippocampal cells. Our aim was also to reveal the subcellular localization where B−TOH undergoes fluorescence

Scheme 1: Lipid (L) Oxidation in the Presence of a Free Radical Initiator (R$^\bullet$) and α-Tocopherol (TOH)[a]

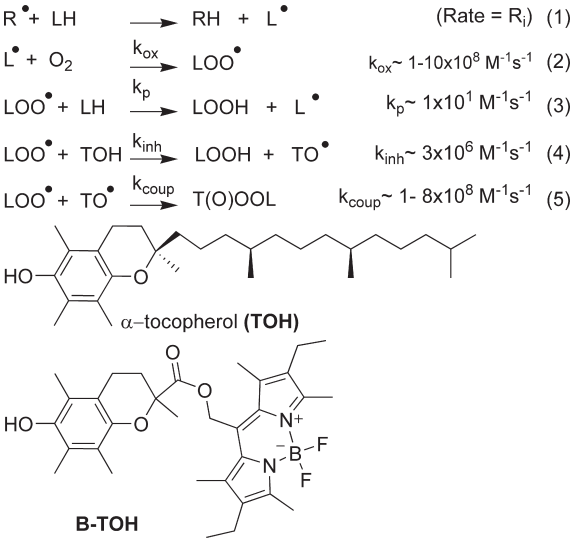

[a] Equation 2 from ref *8*. Equation 3 from ref *9*. Equation 4 from ref *21*. Equation 5 from ref *22*. Also shown are the structures of α-tocopherol (TOH) and B−TOH. Note that eqs 4 and 5 can also be applied to B−TOH (*23*).

enhancement in states of growth factor withdrawal and increased oxidative stress. We explored the consequences that exposure to either *N*,*N*′-dimethyl-4,4′-bipyridinium dichloride (also known as methyl viologen or paraquat) or CdTe nanoparticles has on cells deprived of serum, a state known to induce mild to moderately intense oxidative stress. The choice of these reagents as the source of oxidative stress is ultimately guided by the well-understood effect of methyl viologen on biological systems (*27*−*29*) and by our own interest and ongoing work in assessing and quantifying markers of the toxicity that CdTe nanoparticles exert in biological tissues (*30*−*33*). By employing specific, established dyes for the labeling of multiple cell components, we demonstrate peroxyl radical formation at multiple sites in these cells. Our results underscore the potential of B−TOH as a sensitive and specific probe enabling the molecular imaging of peroxyl radicals in the lipid membrane of live cells.

EXPERIMENTAL PROCEDURES

Preparation and Characterization of B−TOH. B−TOH was prepared as described in the literature (*24*).

Preparation and Characterization of CdTe Nanoparticles. The CdTe nanoparticles (commonly known as quantum dots or QD) used herein are spherical nanoparticles (2.8 nm diameter) consisting of a core rich in metals (cadmium and telluride) and coated with mercaptopropionic acid (MPA), which increases their hydrophilicity and contributes to a negatively charged surface. These nanoparticles were prepared as previously described (*33*). Cells were exposed to CdTe nanoparticles at a concentration of 5 (or 10) *μ*g/mL, which is equivalent to a concentration of 23 (or 46) nM. These particles [$\lambda_{max(em)}$ = 520 nm] are not visible under our cell imaging experimental conditions (low concentration of nanoparticles and 520 nm long pass filter; see below).

B−TOH Partition Coefficient. The partition coefficient of B−TOH between *n*-octanol and water was measured following

previously described methods (*34*). A 1 mM B−TOH solution in a 1:1 *n*-octanol/water mixture was stirred for 2 h at 37 °C. The absorbance of aliquots of the aqueous and organic layer was measured at the maximum of B−TOH absorption, and blanks were prepared with a water-equilibrated *n*-octanol solution and *n*-octanol-equilibrated water solution, respectively. The absorption was used to calculate the B−TOH concentration in water ($[B-TOH]_W$) and in *n*-octanol ($[B-TOH]_O$). The *n*-octanol:water partition coefficient ($P_{O:W}$) is defined according to eq 6:

$$P_{O:W} = \frac{[B-TOH]_O}{[B-TOH]_W} \quad (6)$$

Liposome Preparation. Aqueous solutions (20 mM) in lipids were prepared as follows. First, 135 mg of dimyristoylphosphatidylcholine powder (DMPC, from Avanti Polar Lipids, Alabaster, AL) or 152 mg of egg phosphatidylcholine (EggPC, from Avanti Polar Lipids) was weighed in two dry vials and dissolved with chloroform. The solvent was evaporated while the sample vial was rotated to create a thin film on the vial wall. The films were left under vacuum to remove excess solvent. After 1 h, the aliquots of DMPC and EggPC were hydrated with 10 mL of a pH 7.0, 10 mM phosphate buffer saline solution 150 mM in NaCl, yielding 20 mM DMPC and 20 mM EggPC suspensions, respectively. The lipid suspensions were subjected to five freeze−thaw−sonicate−vortex cycles, where each cycle involved storing the vials with the solutions in dry ice for 4 min followed by a 4 min thawing at 37 °C and culminating in a 4 min sonication at 37 °C. After the fifth cycle, the lipid suspensions were extruded 15 times using an Avanti mini-extruder provided with one 100 nm polycarbonate membrane. Liposomes roughly 100 nm in diameter and each containing ca. 100000 DMPC or EggPC lipids were thus obtained (*35*).

We next embedded B−TOH or PMOH (the precursor to the reporter segment in B−TOH; see structure **1** below) in the liposome membranes. Each sample of DMPC and EggPC was divided into two equal 1.5 mL aliquots. A total of 50 μL of a DMSO solution 80.6 μM in B−TOH was injected into half of the 1.5 mL aliquots of EggPC and DMPC. The other half of the aliquots was injected with 50 μL of a DMSO solution 80.6 μM in PMOH. The DMSO solutions of B−TOH and PMOH were prepared to yield an absorbance of 0.18 upon dilution of 50 μL of a DMSO solution in 1.5 mL of methanol. The same absorbance is expected upon their injection into the liposome dispersion. We obtained a final solution 20 mM in lipids, ca. 200 nM in liposomes, and 2.6 μM in dye (either B−TOH or PMOH). Liposomes were prepared each containing on average 13 fluorophores with a DMPC:fluorophore mole ratio of 7700:1. Under these loading conditions, no fluorescence self-quenching is expected to occur within the bilayer.

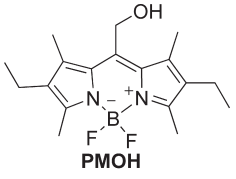

1

To conduct time-resolved studies in a time-correlated single-photon counting setup, the 20 mM liposome solutions were first diluted 20-fold with phosphate buffer (pH 7.0) and then B−TOH or PMOH was added to yield a final solution 1 mM in lipids, ca. 10 nM in liposomes, and 2.6 μM in dye (either B−TOH or PMOH). Solutions were 1 mM in lipids to minimize scattering in the time-correlated single-photon counting setup. Liposomes each containing on average 260 fluorophores, with a DMPC:fluorophore mole ratio of 380:1, were thus obtained.

Liposome Preparation for pH Experiments. DMPC liposomes were prepared in a manner similar to that described above, where lipid films were hydrated with 150 mM NaCl, phosphate buffer saline solutions with pH values of 2.2, 5.6, 8.0, and 10.3, yielding a 20 mM DMPC suspension

Each lipid suspension was subjected to 20 freeze−thaw−sonicate−vortex cycles (no extrusion), where each cycle involved storing the vial with the solution in dry ice for 4 min followed by a 4 min thawing at 37 °C and culminating in a 4 min sonication at 37 °C. Throughout the 20 cycles, the solutions became translucent, indicating a reduction in particle size. As a result of sonication with no extrusion, the liposomes obtained were roughly 100 nm in diameter with a large size distribution (*35*).

We next embedded B−TOH or PMOH in the membrane of the liposomes prepared. Each sample at a given pH was divided into five aliquots of 0.35 mL each. Two aliquots were injected with 15 μL each of a DMSO solution 63.2 μM in B−TOH; two were injected with 15 μL each of a DMSO solution 63.2 μM in PMOH, and a fifth aliquot was left as a blank for the spectroscopy studies. The DMSO solutions of B−TOH and PMOH were prepared to yield an absorbance of 0.18 upon dilution of 15 μL of a DMSO solution in 0.35 mL of methanol. The same absorbance is expected upon their injection into the liposome dispersion. We thus obtained a final solution 20 mM in lipids, 200 nM in liposomes, and 2.6 μM in dye (either B−TOH or PMOH). Liposomes were prepared each containing on average 13 fluorophores, with a DMPC:fluorophore mole ratio of 7700:1. Under these low loading conditions, no fluorescence self-quenching is expected to take place within the bilayer.

Spectroscopy. A Cary Eclipse spectrophotometer with a temperature controller and water circulation was utilized to measure the liposome suspension's fluorescence emission at 565 nm upon excitation at 514 nm using 2.5 nm excitation and emission slits; 1.5 mL of each sample was placed into triangular cuvettes and incubated at 37 °C. To each sample was added 45 μL of a 0.3 M aqueous solution of 2,2′-azobis(2-methylpropionamidine) dihydrochloride (ABAP) (Sigma-Aldrich, Oakville, ON) after equilibration at 37 °C, to yield a final ABAP concentration of 9×10^{-3} M. Fluorescence emission was monitored for 2 h periods at 5 s time intervals to assess the effects of the peroxyl radical on the B−TOH emission enhancement.

The fluorescence lifetime measurements were conducted using a Picoquant Fluotime 200 time-correlated single-photon counting setup employing an LDH 470 ps diode laser (Picoquant) with an excitation wavelength of 470 nm. The laser was controlled with a PDL 800 B picosecond laser driver from Picoquant. The excitation rate was 10 MHz, and the detection frequency was less than 100 kHz. Photons were collected at the magic angle.

A Gemini XS fluorescence well plate reader was utilized to measure the emission from the liposome suspensions; the emission was collected at 565 nm upon excitation at 514 nm. A total of 300 μL of each sample were placed into 20 separate wells and incubated at 37 °C. After equilibration at 37 °C, 15 μL of a 0.18 M aqueous solution of 2,2′-azobis(2-methylpropionamidine) dihydrochloride (ABAP) was added to one sample at each pH, to yield a final ABAP concentration of 9×10^{-3} M.

Fluorescence emission was monitored for 2 h periods at 19 s time intervals to assess the effects of pH and the peroxyl radical on the B−TOH emission enhancement.

Cell Cultures. Rat pheochromocytoma cells (PC12, ATCC) were cultured in RPMI 1640 medium containing 10% FBS (Gibco, Burlington, ON). Cells were maintained at 37 °C (5% CO_2) in a humidified atmosphere. All media contained 1% penicillin-streptomycin and were free of phenol red. Cells were seeded in 24-well plates (Sarstedt, Montreal, QC) at a density of 4×10^4 cells/cm^2, and a density of 10^4 cells/cm^2 was used in eight-well chambers (Laboratory-Tek, Nalge Nunc International, Rochester, NY).

Primary Hippocampal Cell Cultures. The study was performed with the approval of an institutional ethics committee, and all experiments were conducted according to standard stipulated guidelines of animal care. Primary hippocampal neurons and glia from 5-day-old mouse pups (129T2/SV EmsJ, kindly provided by R. Sairam, IRCM, Montreal, QC) were isolated and trypsinized, and the cells were dissociated by repetitive trituration through a Pasteur glass pipet, counted and seeded (5×10^4 cells/well) onto collagen-coated glass coverslips, and grown in a 24-well cell culture plate (Corning) at 37 °C and 5% CO_2 initially in Dulbecco's modified Eagle's medium without phenol red (Invitrogen), 1 mM L-glutamine (Sigma), sodium pyruvate, and PSN (Invitrogen). On the second day in vitro, cells were cultured in Neurobasal A medium without phenol red (Invitrogen) supplemented with 2% (v/v) B-27 supplement (Invitrogen), PSN (Invitrogen), and 1 mM L-glutamine (Sigma) until the eighth day in vitro. On average, four hippocampi per one 24-well plate were required.

Cell Treatment. Cells were washed and maintained in serum-free medium with CdTe nanoparticles (10 μg/mL) for 4 h or 10 μM methyl viologen (Sigma-Aldrich) for 24 h. Primary hippocampal cultures were treated with methyl viologen (10 μM) for 24 h.

Live Cell Imaging. To assess the optimal B−TOH concentration range [$\lambda_{max(abs)}$ = 544 nm; $\lambda_{max(em)}$ = 565 nm in acetonitrile](*23*), an initial screening was done using a wide field fluorescent microsope (Olympus BX-51, Center Valley, PA) at 40× magnification. All other images were acquired with a Zeiss LSM 510 NLO laser scanning confocal inverted microscope at 63× magnification using the Plan Apochromat 63×/1.4 oil objective. Cells were grown on poly-D-lysine HBr (Sigma, P7886) coated eight-well chambers (Laboratory-Tek, Nalge Nunc International) or in 24-well plates with inserted glass coverlips (Fisher 12-545-80) coated with collagen (Sigma, C7661). CdTe nanoparticles or methyl viologen was added to designated wells, and the cells were incubated at 37 °C for either 4 or 24 h. The B−TOH fluorescence enhancement was monitored over time upon excitation with the 488 nm laser line of an Ar^+ laser using an HFT 488 beam splitter and an LP520 emission filter. Detection of lysosomes with Lysotracker DND-99 (500 nM, Molecular Probes) was achieved upon excitation with the 543 nm laser line of a HeNe laser using an HFT 543 beam splitter and an LP560 emission filter. Lipid staining was performed by incubation of cells with Nile Red (1.57 μM) for 10−15 min. Before imaging, cells were washed with PBS or with serum-free medium. Hoechst 33342 (10 μM, 30 min, Molecular Probes; λ_{ex} = 350 nm, and λ_{em} = 461 nm) was used for nuclear staining. No background fluorescence of cells was detected under the settings used. The images (512 × 512 or 1024 × 1024) were recorded upon laser scanning and registering the emission on a photomultiplier tube. Triplicate samples were analyzed in all the imaging experiments. The region scanned was 146.2 μm × 146.2 μm. Figures were created using Adobe Photoshop.

Fluorescent Enhancement Analysis for Time Lapse Experiments. Confocal pictures of PC12 cells stained with B−TOH were analyzed using Image J (version 1.38). Quantification of the fluorescent signal was achieved by calculating the area (%) occupied by B−TOH using an identical threshold of detection for all images. The area (%) of B−TOH fluorescence was normalized to the green autofluorescent signal of PC12 cells and to the number of cells present in each field.

Statistical Analysis. Data were analyzed using SYSTAT 10 (SPSS, Chicago, IL). Statistical significance was determined by Student's *t* tests with Bonferroni correction. Differences were considered significant where $p < 0.05$.

RESULTS

Partition Coefficient. We first measured the partition coefficient ($P_{O:W}$) of the probe between *n*-octanol and water to estimate the affinity of B−TOH for the lipid membrane. A $P_{O:W}$ value of $1.9 \times 10^4 \pm 1 \times 10^3$ was obtained for B−TOH. The value we measured for the B−TOH precursor PMOH was $9 \times 10^3 \pm 1 \times 10^3$. Reported *n*-octanol:water partition coefficients for α-tocopherol range from 3.9×10^{10} to 1.6×10^{12} (*36*). We may thus conclude that B−TOH has a high affinity for the lipid membrane, albeit lower than that of α-tocopherol.

Liposome Studies. We next evaluated the reactivity and emissive properties of B−TOH when embedded in the lipid membrane of liposomes at different pH and in the presence or absence of peroxyl radicals. Control experiments were performed with PMOH. Two different lipid compositions were utilized in preparing the liposomes: dimyristoylphosphatidylcholine (DMPC, saturated fatty acid chains, 14 carbon atoms in length) and egg phosphatidylcholine (EggPC, consisting of a mixture of various phospholipids containing polyunsaturated, unsaturated, and saturated fatty acids with chain lengths of 16 or more carbon atoms, with a saturated to unsaturated mole ratio of 0.82).

In the first set of experiments, we monitored the emission of liposome-embedded B−TOH in the presence of peroxyl radicals generated at a constant rate upon thermolysis of 2,2′-azobis (2-methylpropionamide) dihydrochloride (ABAP) under air (Scheme 2) (*6*, *37*). Liposomes 100 nm in diameter containing on average 13 B−TOH molecules each (lipid:fluorophore mole ratio of 7700:1) were prepared in a pH 7.0 phosphate buffer solution and incubated at 37 °C in the presence of 9 mM ABAP. A linear increase in emission intensity was observed over time for B−TOH when it was embedded in both DMPC and EggPC liposomes. The intensity increase was faster in DMPC liposome solutions than in EggPC liposome solutions, yet in both cases, it leveled off once a ca. 5-fold enhancement had occurred (Figure 1). Upon prolonged exposure to peroxyl radicals, the emission intensity slowly decreased in EggPC liposome solutions; a ca. 9-fold faster drop in intensity was initially observed in DMPC. In the case of control experiments with PMOH, the fluorescence intensity dropped from the start of the experiment, and it qualitatively followed the same rate as that observed for B−TOH samples once they had reached their maximum emission enhancement. In the absence of ABAP, we observed no changes

Scheme 2: Production of Peroxyl Radicals (ROO•) following Thermolysis of ABAP[a]

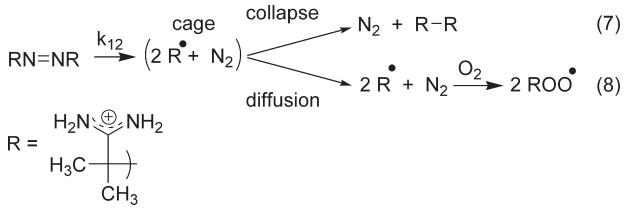

[a] ABAP initially decomposes in a first-order reaction to yield two geminate carbon-centered radicals which may either recombine (eq 7) or diffuse away (eq 8). In air-equilibrated solutions, radicals that escape cage recombination will readily trap molecular oxygen(*38*) to yield two water-soluble peroxyl radicals.

in emission intensity over a period of 2 h for either B−TOH or PMOH (see below).

We also tested what effect, if any, the solution pH has on the reactivity of membrane-embedded B-TOH. DMPC liposomes ca. 100 nm in diameter containing ca. 13 B−TOH or PMOH molecules each (lipid:fluorophore mole ratio of 7700:1) were prepared in various buffers with pH values ranging between 2.2 and 10.3. ABAP was added to one set of solutions at each pH for each dye. A second set was left as a control. In the absence of peroxyl radicals (see Figure S1 of the Supporting Information), we observed that the emission intensity for both dyes remained constant with time at all pH values under these conditions. In the presence of peroxyl radicals, generated at a constant rate upon thermolysis of ABAP at 37 °C in air-saturated solutions (see also Scheme 2), we observed a 4-fold increase in the emission of B−TOH (see Figure S1 of the Supporting Information). In conclusion, neither the reactivity of B−TOH nor its emission properties changed with pH.

In addition to the steady state emission experiments described above, we measured the fluorescence lifetime for B−TOH when embedded within lipid membranes, in an attempt to establish the reason for the lower sensitivity observed in liposome membranes (on:off ratio of 5) as compared to homogeneous solutions in toluene or hexanes (on:off ratio of ≥10). Liposomes 100 nm in diameter containing on average 260 B−TOH or PMOH molecules each (lipid:fluorophore mole ratio of 385:1) were prepared in a pH 7.0 phosphate buffer. Under these loading conditions, no fluorescence self-quenching is expected to take place within the bilayer. Figure 2 shows the fluorescence decay for B−TOH and PMOH when they are embedded in EggPC and DMPC liposomes. Table 1 summarizes the relevant emission decay lifetimes (τ_{decay}). Whereas PMOH has a single-exponential decay in both lipid systems, B−TOH reveals multiexponential decays which can be fitted with a biexponential function as shown in eq 9, where $k_{decay}i$ is the decay rate constant and a_i is the preexponential factor or weight. The average emission decay lifetime for B−TOH is ca. 4-fold smaller than the fluorescence decay lifetime for PMOH.

$$I = a_1 \times \exp^{-(k_{decay}1 \times t)} + a_2 \times \exp^{-(k_{decay}2 \times t)} \quad (9)$$

Live Cell Studies. Our next goal was to apply B−TOH for detection and imaging of peroxyl radicals in the lipid membrane in live cells. We chose as sources of reactive oxygen species methyl viologen, a well-established pro-oxidant agent, and unprotected

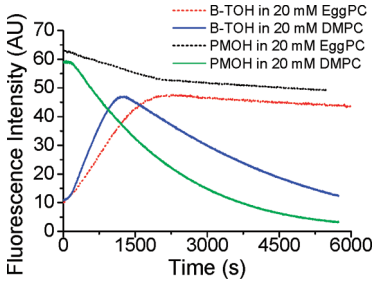

FIGURE 1: Emission intensity time profiles for B−TOH and PMOH embedded in DMPC and EggPC liposome suspensions incubated at 37 °C with ABAP (λ_{exc} = 514 nm; λ_{em} = 565 nm). Samples were air-equilibrated; solutions 2.6 μM in B−TOH, 9 mM in ABAP, and 20 mM in DMPC or 20 mM in EggPC were prepared in a pH 7.0 phosphate buffer. Data points were taken every 5 s.

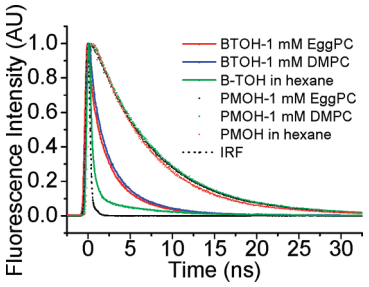

FIGURE 2: Fluorescence decay profiles for 2.6 μM B−TOH and PMOH in 1 mM DMPC or 1 mM EggPC liposomes (λ_{exc} = 470 nm; λ_{em} = 565 nm). Also shown are the decays of PMOH and B−TOH in hexane.

Table 1: Fluorescence Decay Lifetime Values for B−TOH and PMOH Embedded in Lipid Membranes[a]

	lipid	$\tau_{decay}1$ (ns)	a_1	$\tau_{decay}2$ (ns)	a_2	$\langle\tau_{decay}\rangle$ (ns)
PMOH	DMPC	7.27	1	NA	NA	7.27
	EggPC	7.19	1	NA	NA	7.19
	hexanes	6.57[b]	1	NA	NA	6.57
B−TOH	DMPC	1.18	0.52	3.88	0.48	1.8
	EggPC	1.12	0.51	3.63	0.49	1.7
	hexanes	0.44[b]	1	NA	NA	0.44

[a] Herein, $\tau_{decay}i = 1/k_{decay}i$; see eq 9 for a_i and $k_{decay}i$ definitions. [b] From ref *23*.

CdTe nanoparticles known to leak Cd^{2+} into the solution, thus indirectly promoting the formation of ROS (*39*). The choice of these reagents as the source of oxidative stress is ultimately guided by the well-understood effect of methyl viologen on biological systems and by our own interest in assessing and quantifying markers of the toxicity that CdTe nanoparticles exert in biological tissues.

Treatment of PC12 cells with CdTe nanoparticles or methyl viologen in the absence of trophic factors leads to severe oxidative stress and cell death (*33*). We first established the concentration of B−TOH required for the detection of peroxyl radicals in living (unfixed) PC12 cells under optimal and stressed (i.e., serum-starved) conditions using a wide field fluorescence microscope. Herein, a series of B−TOH concentrations were tested (Figure 3A). In PC12 cells deprived of growth factors, there was a marked increase in the B−TOH fluorescence intensity when CdTe nanoparticles, known to enhance oxidative stress in serum-deprived conditions, were added (*33*).

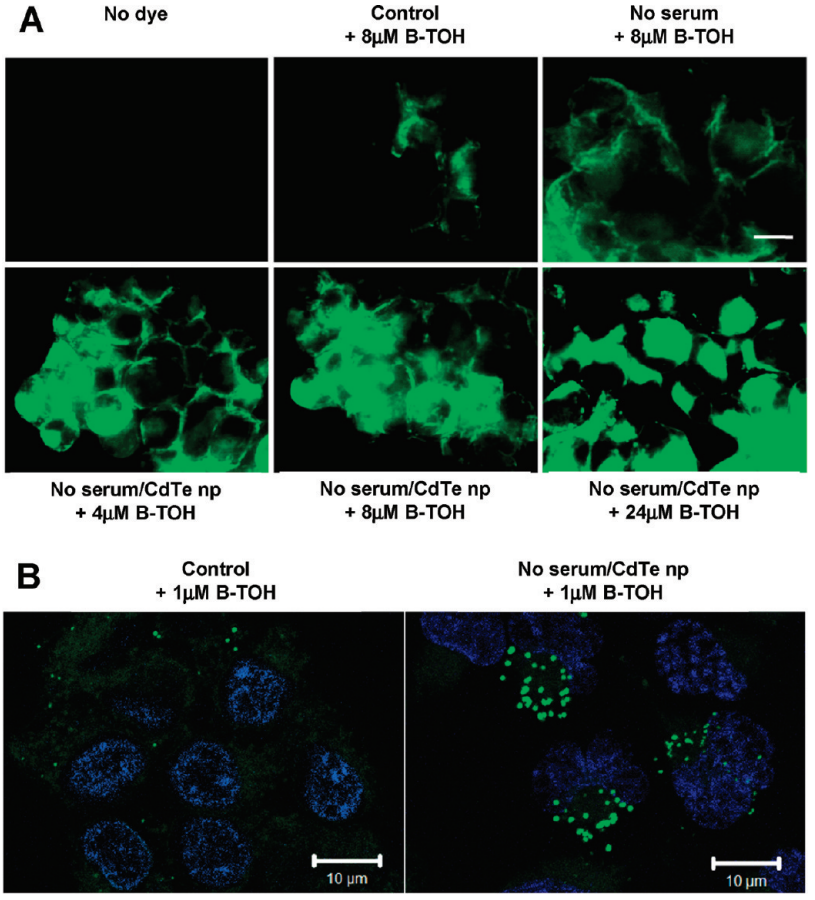

FIGURE 3: Detection of lipid peroxidation with B−TOH under different conditions in PC12 cells. (A) Live adherent PC12 cells were stained with increasing concentrations of B−TOH in the absence of treatment, with a 20 h serum withdrawal, or with a 4 h CdTe np/serum-free (10 μg/mL) treatment. Cell images were taken within 10 min of B−TOH staining. The bar is 20 μm. (B) Confocal micrographs showing B−TOH staining in untreated (left) and CdTe np-treated (right) (10 μg/mL, 4 h) live PC12 cells. Nuclei (blue) were stained with Hoechst 33342 (10 μM) for 30 min. Bars are 10 μm.

A concentration-dependent increase in fluorescence intensity was observed when cells were treated with 4−24 μM B−TOH for 10 min. The presence of peroxyl radicals in cells exposed to CdTe nanoparticles was easily detectable by employing any B−TOH concentration between 4 and 24 μM (Figure 3A). The green fluorescent signal was diffuse within the cells at higher concentrations. This diffuseness could be partly caused by the leakiness of cellular membranes damaged by the CdTe nanoparticles, as demonstrated in our previous studies employing propidium iodide as a label (*33*).

We conducted all subsequent experiments with a concentration of either 1 or 5 μM, since the signal saturated above 8 μM B−TOH (see Figure 3A). These experiments were conducted using a confocal microscope to gain a detailed spatial resolution in terms of probe localization in membranes and organelles (Figure 3B). Confocal micrographs from these studies show that PC12 cells stressed with CdTe nanoparticles (10 μg/mL, 4 h) become highly emissive at the membranes of multiple intracellular organelles (Figure 3B).

To examine the dynamics and quantify the relative amount of lipid peroxyl radicals in live PC12 cells, we performed time lapse experiments with the confocal microscope. PC12 cells were deprived of serum overnight, and one fraction of the cells was additionally treated with CdTe nanoparticles (5 μg/mL) for 4 h. Subsequently, each set of cells was incubated with B−TOH (5 μM) for up to 18 min. Excitation of B−TOH at 488 nm was performed to image the cells. For those cells that were incubated overnight without trophic factors (serum-deprived), we observed that the fluorescence of B−TOH increased in a time-dependent manner (Figures 4A and 5). Additionally, treating serum-deprived cells with CdTe nanoparticles caused an even larger amplification in the fluorescence of B−TOH (Figures 4B and 5). Following an 18 min incubation, we observed a 19-fold increase (relative to autofluorescence) in the B−TOH emission signal for the CdTe nanoparticle-treated cells, compared to 15-fold in the serum-free (no CdTe nanoparticle) condition (Figure 5). The induction of lipid peroxidation by CdTe nanoparticles was partially inhibited by the addition of a commonly used antioxidant molecule, *N*-acetylcysteine (NAC) (*30*, *33*). Treatment with NAC for 2 h prior to CdTe nanoparticle addition attenuated the magnitude of the B−TOH fluorescence enhancement observed with the CdTe nanoparticles (panel B vs panel C of Figure 4; also see Figure 5). At 18 min, the increase in the magnitude of the B−TOH signal in NAC-treated samples was 15-fold (relative to autofluorescence), compared to 19-fold in CdTe nanoparticle-treated cells. Finally, at 18 min the increase in the magnitude of the B−TOH signal for control cells incubated with serum was 5-fold. A similar result was obtained for cells incubated with serum but treated with CdTe nanoparticles. Arguably, the small increase in intensity is due to low levels of lipid peroxidation in cells cultured in serum-containing media. The increase may also be in part due to slow uptake of B−TOH via the endocytic process, what has been shown to take place over several minutes for labeled α-tocopherol in hepatocytes (*40*).

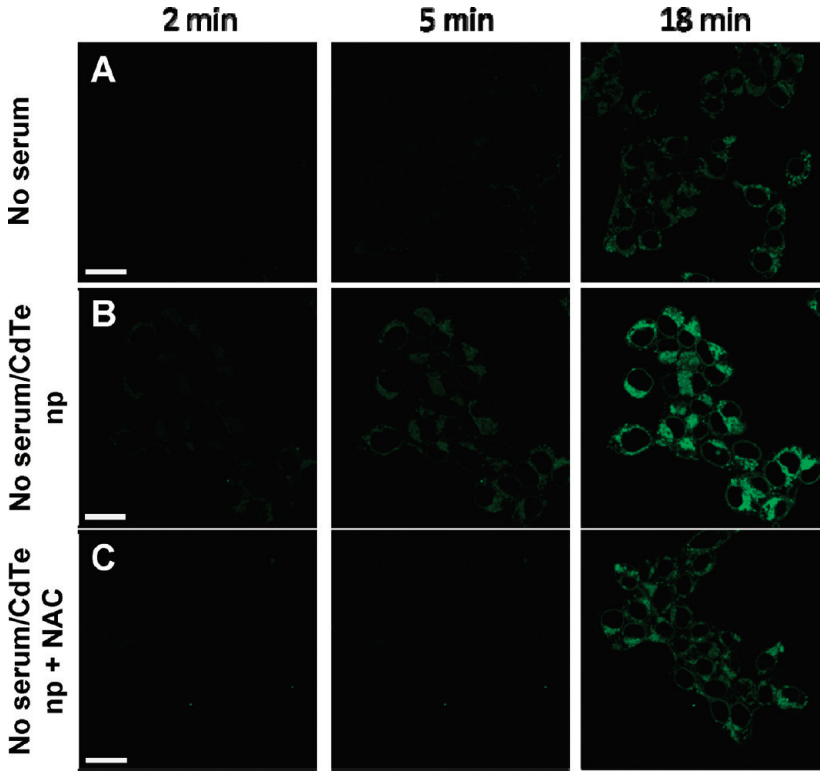

FIGURE 4: B−TOH as a sensor for dynamic changes in peroxyl radical formation in PC12 cells. The top three panels illustrate the time-dependent increase in B−TOH fluorescence for (A) serum-deprived PC12 cells, (B) serum-deprived and CdTe np-treated PC12 cells, and (C) serum-deprived, CdTe np-treated, and NAC-treated PC12 cells. The bar is 20 μm in all cases. PC12 cells were deprived of serum overnight and treated with CdTe np (5 μg/mL) for 4 h. NAC (2 mM) was added to the cell culture medium 2 h prior to the addition of CdTe np. Cells were then incubated with B−TOH (5 μM) for the indicated periods of time.

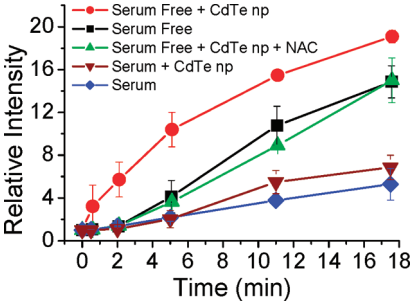

FIGURE 5: B−TOH fluorescence intensity vs time plot recorded for PC12 cells that were (circles) deprived of serum and treated with CdTe np, (squares) deprived of serum, (upward-pointing triangles) deprived of serum, treated with CdTe np, and treated with NAC, (downward-pointing triangles) incubated with serum and treated with CdTe np, and (diamonds) incubated with serum. The fluorescence intensity was normalized by the number of cells present in each field of view, and the increase in B−TOH emission intensity is normalized to the autofluorescence of the cells (emission at $t = 0$). *Y*-Axis values represent means of at least two independent experiments. PC12 cells were deprived of serum overnight and treated with CdTe np (5 μg/mL) for 4 h. NAC (2 mM) was added to the cell culture medium 2 h prior to the addition of CdTe np. Cells were then incubated with B−TOH (5 μM) for the indicated periods of time.

Altogether, these experiments report on the relative concentration of lipid peroxyl radicals in live cells under various treatments and conditions and underscore that changes in the extent of lipid peroxidation can be measured with B−TOH.

We additionally examined the presence of peroxyl radicals in the membranes of different subcellular structures of growth factor-deprived PC12 cells. Imaging was done with the confocal microscope upon staining with B−TOH (1 μM for 10 min) and with Nile Red (1.57 μM for 10 min), a commonly used dye for labeling neutral lipids and phospholipids in living and fixed cells (*41*) (Figure 6).

Under growth factor deprivation conditions, B−TOH localized in ringlike structures in PC12 cells where Nile Red also localized. The observed ringlike structures are reminiscent of a specific vesicular structure, the autophagosomes, which typically develop in cells under oxidative stress and starvation (*42*). We then examined peroxyl radical formation on another subcellular compartment, the lysosome. Lysotracker Red DND-99 is an acidotropic dye used to stain lysosomes. The colocalization of oxidized B−TOH (1 μM for 10 min) and of Lysotracker Red DND-99 (500 nM for 3 min) ultimately reveals the presence of peroxyl radicals in lysosomes (Figure 7). B−TOH and Lysotracker labeling in mouse hippocampal cultures stressed with methyl viologen (10 μM for 24 h; see Figure 7) conveys a similar message: B−TOH reports on the presence of lipid peroxyl radicals in lysosomes of live cells under oxidative stress and growth factor deprivation.

DISCUSSION

Liposome Studies. The observed fluorescence enhancement of B−TOH upon reaction with peroxyl radicals when embedded in either liposomes or cellular lipid organelles is consistent with the B−TOH molecular mechanism of action. The scavenging of two lipid peroxyl radicals by B−TOH, concomitant with the oxidation of the chromanol head in the receptor segment, deactivates the PeT quenching mechanism (off state), leading to emission enhancement (on state) (*23*, *24*). We observed no pH dependence for the B−TOH fluorescence enhancement when it was embedded within liposomes; we can thus rule out any

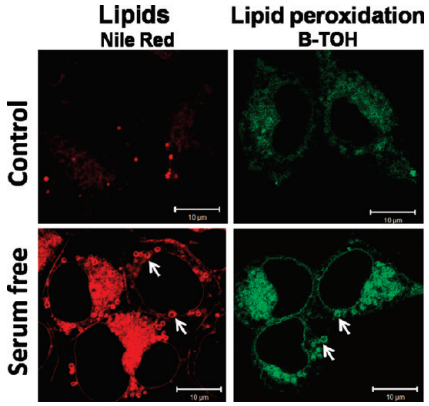

FIGURE 6: Detection of peroxyl radicals by B−TOH and of acidic cytoplasmic compartments by staining with Lysotracker DND-99. Living PC12 cells in serum-containing and serum-free medium (24 h) were stained with Nile Red (1.57 μM for 10 min) for lipids and with B−TOH (1 μM for 10 min) for peroxyl radicals. Arrows indicate ringlike structures reminiscent of autophagic vacuoles. The bars are 10 μm.

contribution arising from the hydrolysis of the ester linkage between the receptor and reporter end. The fluorescence enhancement is due solely to the reaction of B−TOH with peroxyl radicals.

Under the experimental conditions employed here, the emission enhancement is ca. 5-fold in the presence of peroxyl radicals produced upon ABAP thermolysis under air. This value is lower than that anticipated from homogeneous solution studies, where enhancements of ca. 10-fold have been measured. We thus conducted fluorescence lifetime studies on B−TOH and PMOH to elucidate the photophysical behavior of the probe within the lipid media.

PMOH decay is monoexponential, and its characteristic decay rate constant is similar to that determined in homogeneous solutions (see Table 1) (*23*). This is not surprising since the photophysical properties of BODIPY fluorophores do not show a significant solvent effect (*43*). B−TOH undergoes multiexponential fluorescence decay when intercalated within the lipid membrane, where the decay rate can be fit by a minimum of two exponential terms. Further, the average fluorescence lifetime is significantly larger than that for B−TOH in homogeneous solution (1.7 and 0.44 ns, respectively).

One may show (see eq 10) that given the average fluorescence lifetime (τ_{decay}) for B−TOH is ca. 4-fold smaller than the emission decay lifetime for PMOH in the lipid membrane, and considering that the BODIPY radiative lifetime (τ_r) is not affected by the solvent (*43*), the intensity enhancement for B−TOH upon oxidation by peroxyl radicals should not surpass a value of 4 or 4.5, consistent with our experimental observations.

$$\phi_f = \frac{\tau_{decay}}{\tau_r} \tag{10}$$

The multiexponential behavior in B−TOH decay is consistent with the probe experiencing a range of environments within the lipid bilayer. Motion restriction of the receptor−reporter segments provides a plausible explanation for B−TOH's larger τ_{decay} during its off state in lipid membrane versus that in homogeneous solution, whereupon one may foresee that the receptor and reporter segments are required to mutually approach for intramolecular electron transfer to occur. Interestingly, in EggPC membranes, the B−TOH fluorescence lifetime is somewhat shorter than in DMPC membranes; this most probably reflects a more fluid environment for the probe in the former case (*44*).

Having discussed the photophysics for B−TOH and PMOH when they were membrane-intercalated, we next address its reactivity in model lipid membranes. The linear growth in intensity (and consumption of B−TOH) over time is consistent with a rate law which is zero-order with respect to the receptor (antioxidant) segment in B−TOH. By analogy to our previous studies in homogeneous solution, we assign the initial increase in intensity to the two-radical oxidation of the chromanol head in B−TOH into a chromanone or chromoquinone (*23*).

Significant information about the probe reactivity may be obtained from our studies under controlled generation of peroxyl radicals (*6*, *37*, *45*). According to eq 11, at any given time t one may estimate the total yield of peroxyl radicals on the basis of the rate of thermolysis of ABAP at 37 °C (k_{12}), the fraction of geminate radicals that escape recombination (e), and the initial concentration of ABAP (see Scheme 2, eqs 7 and 8).

$$[ROO^\bullet]_t = 2ek_{12}[ABAP]t \tag{11}$$

One may then estimate the time for complete consumption of the probe (or induction period τ) and compare it to the experimental values (see eq 12). Our estimates yield a τ value of 517 s under our experimental conditions (2.6 μM B−TOH and 9 mM ABAP at 37 °C). A main assumption in the above estimate is that all peroxyl radicals formed are scavenged by B−TOH, i.e., $2[B-TOH]_0 = [ROO^\bullet]_t$, where we utilized a stoichiometric factor of 2 for B−TOH scavenging of peroxyl radicals (see also eqs 4 and 5 in Scheme 1) (*23*). We further used the value for the escape fraction $e = 0.43$ obtained for ABAP in the presence of multilamellar liposomes prepared from dilinoleoylphosphatidylcholine (DLPC)(*6*) and the rate constant of thermolysis ($k_{12} = 1.3 \times 10^{-6}$) at 37 °C in buffer solution (*37*).

$$\tau = \frac{2[B-TOH]}{2ek_{12}[ABAP]} \tag{12}$$

Experimentally, one may obtain the time for B−TOH consumption from the analysis of the time profile for the emission intensity growth and subsequent decay (*44*). We obtained the following values: $\tau = 1.0 \times 10^3$ s in DMPC and $\tau = 1.6 \times 10^3$ s in EggPC. These values are significantly larger than the theoretical estimate of 517 s.

We may conclude on the basis of the observations described above that the probe is moderately sensitive to the membrane system under study, where we observe differences in the rate of B−TOH consumption by water-soluble peroxyl radicals. A plausible explanation for the larger than expected τ measured in EggPC and DMPC is the low availability of B−TOH to the water-soluble peroxyl radicals (*44*). A low B−TOH availability will in turn lead to a larger fraction of the water-soluble radicals undergoing bimolecular self-reaction to yield nonradical products (*45*). Interestingly, in DMPC liposomes, the larger rate of intensity growth recorded upon free radical scavenging by the B−TOH receptor segment correlates with the faster rate of intensity drop once the receptor segment in B−TOH is consumed. Arguably, the intercalation within DMPC and EggPC is different for the lipophilic fluorophore (either PMOH or B−TOH). On the basis of the results described above, the fluorophore lies more exposed to water-soluble peroxyl radicals in DMPC than in EggPC; i.e., B−TOH and PMOH penetrate more readily in EggPC than in DMPC membranes. In any event, B−TOH is

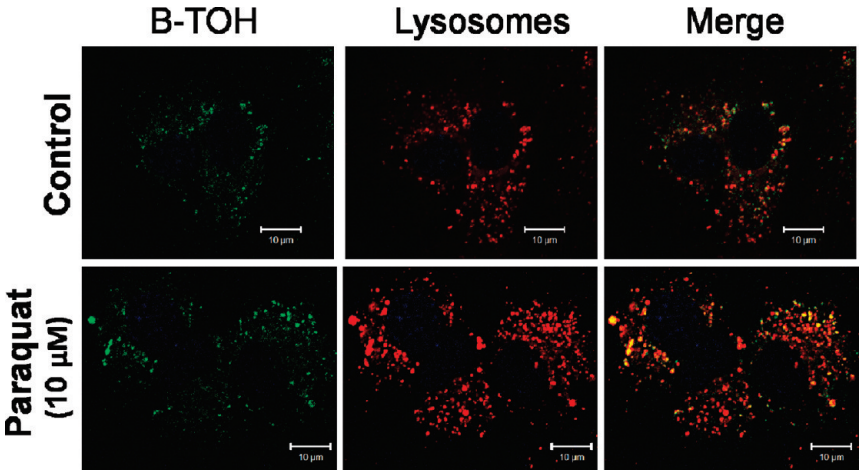

FIGURE 7: Lipid peroxidation and acidic cytoplasmic compartments in primary culture of mouse hippocampus. Lipid peroxidation was induced by treating hippocampal neural cultures with methyl viologen (10 μM) for 24 h. Lipid peroxidation is colored green and was detected by B−TOH (1 μM for 10 min), and lysosomes (red) were detected using Lysotracker DND-99 (500 nM for 3 min). Hoechst (10 μM for 30 min) staining reveals nuclei (blue). The bars are 10 μm.

membrane-embedded in both EggPC and DMPC, which can be concluded both from the large octanol:water partition coefficient and from the observed emission for both probes in the lipid media [B−TOH and PMOH are nonemissive in aqueous dispersions, where they most probably form nonemissive aggregates (data not shown)].

A considerable body of work has gone into gaining a molecular-level understanding of the interaction of α-tocopherol with lipids in the lipid membranes. Major aspects of this topic have been recently reviewed (*46*−*48*). Three models have been proposed to describe where tocopherols reside within membranes (*49*) and where differences in the models arise on pinpointing the depth of α-tocopherol location within the membrane. Discrepancies are the result both of the different experimental methods employed and the type of lipids used in the studies. A prevailing picture is the one in which the chromanol is recessed into the membrane, possibly involved in hydrogen bonding with either phosphate oxygen or acyl ester oxygen atoms in the lipid (*46*). Interestingly, it has recently been observed that whereas in palmitolyloleoylphosphatidylcholine (POPC) tocopherol is found high in the membrane, in dioleoylphosphatidylcholine (DOPC) it sits much deeper. It has been proposed along those lines that α-tocopherol penetration depth may increase with a greater degree of unsaturation (*46*). In related work, Maggio et al. described the penetration of α-tocopherol and derivatives into monolayers at the air−water interface (*50*). They found that α-tocopherol and derivatives penetrate more readily into monolayers prepared from phospholipids with unsaturated fatty acid substituents than into monolayers prepared from their saturated counterparts. The presence of unsaturated phospholipids in mixed saturated−unsaturated lipid mixtures was also shown to facilitate the penetration of α-tocopherol and its derivatives (*50*). When discussing the lipophilic tail in B−TOH, we may further point out that BODIPY preferentially partitions in membranes rich in unsaturated fatty acids as compared to membranes rich in saturated ones. This phenomenon has been exploited for imaging lipid domains within lipid bilayers (*51*).

Our results on the reactivity of B−TOH and its position within the membrane are in line with the results recently reviewed; i.e., we observe a larger penetration depth by B−TOH in EggPC than in DMPC (*46*). We note, however, that significant differences exist in the lipophilic tail in B−TOH versus that in α-tocopherol. Nonetheless, our data emphasize how important the surrounding lipid structure may be in determining the peroxyl radical scavenging ability of α-tocopherol and other members of the vitamin E family, a key concept in assessing vitamin E antioxidant activity (*46*).

Live Cell Studies. In studies at the cellular level, B−TOH was able to report both methyl viologen- and CdTe nanoparticle-induced lipid peroxidation in a concentration-dependent manner in PC12 cells. Methyl viologen catalyzes the reduction of molecular oxygen to water, yielding various ROS intermediates along the way (*27*). Our previous studies indicate that CdTe nanoparticles induce ROS formation and produce lipid peroxidation in several cell types, namely, in PC12 (pheochromocytoma) and SH-SY5Y (neuroblastoma) cells (*30*, *32*). Cadmium nanoparticles, like the ones used in our experiments, release Cd^{2+} ions from their core when they are degraded. Whereas Cd^{2+} is unable to directly produce ROS, it acts by displacing iron and copper from various proteins (*29*); the resulting free iron and copper ions in turn take part in a metal-catalyzed reduction of oxygen into water with the formation of various ROS intermediates along the way (*28*). Cd^{2+} ions produce ROS by interfering with antioxidant enzymes and by causing mitochondrial membrane dysfunction (*52*, *53*). ROS generated by free Cd^{2+} could be responsible for initiating or reinforcing the propagation of lipid peroxidation in cells (*52*).

Labeling with Nile Red clearly shows vesicular structures with double membranes in cells exposed to nutrient deprivation. Some of these double-membrane structures are stained with B−TOH, suggesting that lipid peroxidation may occur on lipidic membrane vacuoles. The localization of fluorescent B−TOH within lysosomes would be consistent with the high content of α-tocopherol that has been reported to exist within these organelles. Indeed, in rat liver subcellular membranes, the α-tocopherol:phospholipid mole ratio was found to be 1:65 in lysosomes and Golgi membranes, which is 1 order of magnitude larger than in mithochondria, microsomes, or the nuclear fraction (*47*, *54*). Experiments with labeled α-tocopherol have also shown that it is incorporated via an endocytic process in hepatocytes, where shortly following uptake it is found within the lysosomes (*40*). Whereas lysosome staining by B−TOH (visible following oxidation of B−TOH by peroxyl radicals) is indeed a reasonable assumption, this needs to be proved by

detecting colocalization of B−TOH with lysosomal resident proteins, such as lysosomal-associated membrane protein-1 (LAMP1) (*55*).

Pretreatment with the antioxidant NAC significantly reduced the magnitude of the B−TOH signal in CdTe nanoparticle-treated PC12 cells, suggesting a protective role of NAC against CdTe nanoparticle-induced lipid peroxidation. The protective effects of NAC against CdTe nanoparticle-induced cytotoxicity have been demonstrated in several cell lines by several groups (*30*, *32*). More specifically, pretreatment of cells with NAC prevented significant enhancement of lipid peroxidation following CdTe nanoparticle treatment (*30*), and it reduced the levels of lipid peroxidation markers [e.g., 4-hydroxy-2-nonenal (HNE)] in skin fibroblasts from Alzheimer's disease (AD) patients (*56*).

CONCLUSIONS

Our studies in liposomes and live cells underscore the potential of B−TOH for molecular imaging of lipid peroxyl radicals in the membranes of live cells. Numerous studies have shown that reactive oxygen species accumulate during aging and that they contribute to neurodegenerative disorders. In this study, B−TOH has been successfully used to track the formation of lipid peroxides in primary hippocampal neural cultures from mice following an oxidative insult, as illustrated in Figure 7. This example clearly demonstrates the potential application of B−TOH as a novel sensor suitable for peroxyl radical detection in model cells and eventually in tissues under both physiological and pathological conditions.

Our results show the following. (i) There is a 5-fold increase in emission upon reaction of lipid-intercalated B−TOH with peroxyl radicals. (ii) B−TOH is very reactive and readily traps a large fraction of peroxyl radicals when embedded within lipid membranes. (iii) B−TOH can be used as a fluorescent biomarker to examine the relative concentration of lipid peroxyl radicals in live cells under various treatments and conditions. (iv) It is possible to detect lipid peroxyl radicals in different subcellular structures, including lipid-rich vesicles and lysosomes when cells are deprived of nutrient and trophic factors.

The critical importance of monitoring lipid peroxyl radicals cannot be overemphasized. Whereas the chemistry of lipid peroxyl radicals is becoming well understood, it is unclear how this translates into cellular mechanisms. Imaging studies with specific sensors will help provide a molecular-level understanding of the role lipid peroxyl radicals play in the cellular mechanisms of pathologies and signaling. We strongly believe that our results presented herein are a step forward in this direction.

ACKNOWLEDGMENT

We thank Alexandre Moquin for the preparation and characterization of CdTe nanoparticles and Jacynthe Laliberté for her help with the confocal microscopy experiments. We also thank Pascal Beauchamp and Dr. Imed Gallouzi for assistance in live imaging experiments with the fluorescence microscope and the Center of Self Assembled Chemical Structures (CSACS/CRMAA) for use of the facilities.

SUPPORTING INFORMATION AVAILABLE

Steady state fluorescence experiments performed with B−TOH intercalated within DMPC bilayers under various pH conditions. This material is available free of charge via the Internet at http://pubs.acs.org.

REFERENCES

1. Halliwell, B., and Gutteridge, J. M. C. (2007) *Free Radicals in Biology and Medicine* , 4th ed., Oxford University Press, Oxford.
2. (a) Winterbourn, C. C. (2008) Reconciling the chemistry and biology of reactive oxygen species. *Nat. Chem. Biol. 4*, 278–286. (b) Droge, W. (2002) Free Radicals in the Physiological Control of Cell Function. *Physiol. Rev. 82*, 47–95. (c) Apel, K., and Hirt, H. (2004) Reactive Oxygen Species: Metabolism, Oxidative Stress, and Signal Transduction. *Annu. Rev. Plant Biol. 55*, 373–399. (d) Rhee, S. G. (2006) Cell Signaling: H_2O_2, a Necessary Evil for Cell Signaling. *Science 312*, 1882–1883. (e) Lesser, M. P. (2006) Oxidative Stress in Marine Environments: Biochemistry and Physiological Ecology. *Annu. Rev. Physiol. 68*, 253–278.
3. Kagan, V. E., and Quinn, P. J. (2004) Toward Oxidative Lipidomics of Cell Signaling. *Antioxid. Redox Signaling 6*, 199–202.
4. West, J. D., and Marnett, L. J. (2006) Endogenous Reactive Intermediates as Modulators of Cell Signaling and Cell Death. *Chem. Res. Toxicol. 19*, 173–194.
5. (a) Barclay, L. R. C., and Ingold, K. U. (1981) Autoxidation of biological molecules. 2. Autoxidation of a model membrane. Comparison of the autoxidation of egg lecithin phosphatidylcholine in water and in chlorobenzene. *J. Am. Chem. Soc. 103*, 6478–6485. (b) Cosgrove, J., Church, D., and Pryor, W. (1987) The kinetics of the autoxidation of polyunsaturated fatty acids. *Lipids 22*, 299–304. (c) Yamamoto, Y., Haga, S., Niki, E., and Kamiya, Y. (1984) Oxidation of lipids. V. Oxidation of methyl linoleate in aqueous dispersion. *Bull. Chem. Soc. Jpn. 57*, 1260–1264.
6. Barclay, L. R. C., Locke, S. J., MacNeil, J. M., VanKessel, J., Burton, G. W., and Ingold, K. U. (1984) Autoxidation of micelles and model membranes. Quantitative kinetic measurements can be made by using either water-soluble or lipid-soluble initiators with water-soluble or lipid-soluble chain-breaking antioxidants. *J. Am. Chem. Soc. 106*, 2479–2481.
7. Porter, N. A. (1986) Mechanisms for the autoxidation of polyunsaturated lipids. *Acc. Chem. Res. 19*, 262–268.
8. Hasegawa, K., and Patterson, L. K. (1978) Pulse radiolysis studies in model lipid systems: Formation and behavior of peroxy radicals in fatty acids. *Photochem. Photobiol. 28*, 817–823.
9. Niki, E., and Noguchi, N. (2004) Dynamics of Antioxidant Action of Vitamin E. *Acc. Chem. Res. 37*, 45–51.
10. (a) Barclay, L. R. C. (1993) Model biomembranes: Quantitative studies of peroxidation, antioxidant action, partitioning, and oxidative stress. *Can. J. Chem. 71*, 1–16. (b) Chatgilialoglu, C., and Ferreri, C. (2005) Trans Lipids: The Free Radical Path. *Acc. Chem. Res. 38*, 441–448. (c) Chatgilialoglu, C., Ferreri, C., Ballestri, M., Mulazzani, Q. G., and Landi, L. (2000) Cis-trans Isomerization of Monounsaturated Fatty Acid Residues in Phospholipids by Thiyl Radicals. *J. Am. Chem. Soc. 122*, 4593–4601.
11. Sun, M., and Salomon, R. G. (2004) Oxidative Fragmentation of Hydroxy Octadecadienoates Generates Biologically Active γ-Hydroxyalkenals. *J. Am. Chem. Soc. 126*, 5699–5708.
12. Esterbauer, H., Schaur, R. J., and Zollner, H. (1991) Chemistry and biochemistry of 4-hydroxynonenal, malonaldehyde and related aldehydes. *Free Radical Biol. Med. 11*, 81–128.
13. Borst, J. W., Visser, N. V., Kouptsova, O., and Visser, A. J. W. G. (2000) Oxidation of unsaturated phospholipids in membrane bilayer mixtures is accompanied by membrane fluidity changes. *Biochim. Biophys. Acta 1487*, 61–73.
14. Yuan, J., Hira, S. M., Strouse, G. F., and Hirst, L. S. (2008) Lipid Bilayer Discs and Banded Tubules: Photoinduced Lipid Sorting in Ternary Mixtures. *J. Am. Chem. Soc. 130*, 2067–2072.
15. Barnham, K. J., Masters, C. L., and Bush, A. I. (2004) Neurodegenerative diseases and oxidative stress. *Nat. Rev. Drug Discovery 3*, 205–214.
16. Bowry, V. W., and Ingold, K. U. (1999) The Unexpected Role of Vitamin E (α-Tocopherol) in the Peroxidation of Human Low-density Lipoprotein. *Acc. Chem. Res. 32*, 27–34.
17. Kagan, V. E., Fabisiak, J. P., Shvedova, A. A., Tyurina, Y. Y., Tyurin, V. A., Schor, N. F., and Kawai, K. (2000) Oxidative signaling pathway for externalization of plasma membrane phosphatidylserine during apoptosis. *FEBS Lett. 477*, 1–7.
18. Berliner, J. A., and Zimman, A. (2007) Future of Toxicology-Lipidomics, an Important Emerging Area for Toxicologists: Focus on Lipid Oxidation Products. *Chem. Res. Toxicol. 20*, 849–853.
19. Kagan, V. E., Tyurin, V. A., Jiang, J., Tyurina, Y. Y., Ritov, V. B., Amoscato, A. A., Osipov, A. N., Belikova, N. A., Kapralov, A. A., Kini, V., Vlasova, I. I., Zhao, Q., Zou, M., Di, P., Svistunenko, D. A., Kurnikov, I. V., and Borisenko, G. G. (2005) Cytochrome c acts as a cardiolipin oxygenase required for release of proapoptotic factors. *Nat. Chem. Biol. 1*, 223–232.

20. Kagan, V. E., Fabisiak, J. P., Shvedova, A. A., Tyurina, Y. Y., Tyurin, V. A., Schor, N. F., and Kawai, K. (2000) Oxidative signaling pathway for externalization of plasma membrane phosphatidylserine during apoptosis. *FEBS Lett. 477*, 1–7.
21. Burton, G. W., and Ingold, K. U. (1986) Vitamin E: Application of the principles of physical organic chemistry to the exploration of its structure and function. *Acc. Chem. Res. 19*, 194–201.
22. Jonsson, M., Lind, J., Reitberger, T., Eriksen, T. E., and Merenyi, G. (1993) Free radical combination reactions involving phenoxyl radicals. *J. Phys. Chem. 97*, 8229–8233.
23. Krumova, K., Oleynik, P., Karam, P., and Cosa, G. (2009) Phenol-based Lipophilic Fluorescent Antioxidant Indicators: a Rational Approach. *J. Org. Chem. 74*, 3641–3651.
24. Oleynik, P., Ishihara, Y., and Cosa, G. (2007) Design and Synthesis of a BODIPY-α-Tocopherol Adduct for Use as an Off/On Fluorescent Antioxidant Indicator. *J. Am. Chem. Soc. 129*, 1842–1843.
25. Burton, G. W., Doba, T., Gabe, E., Hughes, L., Lee, F. L., Prasad, L., and Ingold, K. U. (1985) Autoxidation of biological molecules. 4. Maximizing the antioxidant activity of phenols. *J. Am. Chem. Soc. 107*, 7053–7065.
26. de Silva, A. P., Gunaratne, H. Q. N., Gunnlaugsson, T., Huxley, A. J. M., McCoy, C. P., Rademacher, J. T., and Rice, T. E. (1997) Signaling Recognition Events with Fluorescent Sensors and Switches. *Chem. Rev. 97*, 1515–1566.
27. (a) Cadenas, E. (1989) Biochemistry of Oxygen Toxicity. *Annu. Rev. Biochem. 58*, 79–110. (b) Farrington, J. A., Ebert, M., Land, E. J., and Fletcher, K. (1973) Bipyridylium quaternary salts and related compounds. V. Pulse radiolysis studies of the reaction of paraquat radical with oxygen. Implications for the mode of action of bipyridyl herbicides. *Biochim. Biophys. Acta 314*, 372–381.
28. (a) Lai, C.-S., and Piette, L. H. (1978) Spin-trapping studies of hydroxyl radical production involved in lipid peroxidation. *Arch. Biochem. Biophys. 190*, 27–38. (b) Halliwell, B., and Gutteridge, J. M. C. (1992) Biologically relevant metal ion-dependent hydroxyl radical generation An update. *FEBS Lett. 307*, 108–112. (c) Casalino, E., Sblano, C., and Landriscina, C. (1997) Enzyme Activity Alteration by Cadmium Administration to Rats: The Possibility of Iron Involvement in Lipid Peroxidation. *Arch. Biochem. Biophys. 346*, 171–179.
29. Price, D. J., and Joshi, J. G. (1983) Ferritin. Binding of beryllium and other divalent metal ions. *J. Biol. Chem. 258*, 10873–10880.
30. Choi, A. O., Cho, S. J., Desbarats, J., Lovric, J., and Maysinger, D. (2007) Quantum dot-induced cell death involves Fas upregulation and lipid peroxidation in human neuroblastoma cells. *J. Nanobiotechnol. 5*, 1.
31. Funnell, W. R., and Maysinger, D. (2006) Three-dimensional reconstruction of cell nuclei, internalized quantum dots and sites of lipid peroxidation. *J. Nanobiotechnol. 4*, 10.
32. Lovric, J., Bazzi, H. S., Cuie, Y., Fortin, G. R., Winnik, F. M., and Maysinger, D. (2005) Differences in subcellular distribution and toxicity of green and red emitting CdTe quantum dots. *J. Mol. Med. 83*, 377–385.
33. Lovric, J., Cho, S. J., Winnik, F. M., and Maysinger, D. (2005) Unmodified cadmium telluride quantum dots induce reactive oxygen species formation leading to multiple organelle damage and cell death. *Chem. Biol. 12*, 1227–1234.
34. Liao, K. l., and Yin, M. C. (2000) Individual and Combined Antioxidant Effects of Seven Phenolic Agents in Human Erythrocyte Membrane Ghosts and Phosphatidylcholine Liposome Systems: Importance of the Partition Coefficient. *J. Agric. Food Chem. 48*, 2266–2270.
35. Torchilin, V. P., and Weissig, V., Eds. (2003) *Liposomes* , 2nd ed., Vol. *264*, Oxford University Press Inc., New York.
36. (a) Tafazoli, S., Wright, J. S., and O'Brien, P. J. (2005) Prooxidant and Antioxidant Activity of Vitamin E Analogues and Troglitazone. *Chem. Res. Toxicol. 18*, 1567–1574. (b) Cooper, D. A., Webb, D. R., and Peters, J. C. (1997) Evaluation of the Potential for Olestra To Affect the Availability of Dietary Phytochemicals. *J. Nutr. 127*, 1699S.
37. Bedard, L., Young, M. J., Hall, D., Paul, T., and Ingold, K. U. (2001) Quantitative Studies on the Peroxidation of Human Low-Density Lipoprotein Initiated by Superoxide and by Charged and Neutral Alkylperoxyl Radicals. *J. Am. Chem. Soc. 123*, 12439–12448.
38. Maillard, B., Ingold, K. U., and Scaiano, J. C. (1983) Rate constants for the reactions of free radicals with oxygen in solution. *J. Am. Chem. Soc. 105*, 5095–5099.
39. Valko, M., Rhodes, C. J., Moncol, J., Izakovic, M., and Mazur, M. (2006) Free radicals, metals and antioxidants in oxidative stress-induced cancer. *Chem.-Biol. Interact. 160*, 1–40.
40. Qian, J., Morley, S., Wilson, K., Nava, P., Atkinson, J., and Manor, D. (2005) Intracellular trafficking of vitamin E in hepatocytes: The role of tocopherol transfer protein. *J. Lipid Res. 46*, 2072–2082.
41. Greenspan, P., Mayer, E. P., and Fowler, S. D. (1985) Nile red: A selective fluorescent stain for intracellular lipid droplets. *J. Cell Biol. 100*, 965–973.
42. (a) Terman, A., Gustafsson, B., and Brunk, U. T. (2007) Autophagy, organelles and ageing. *J. Pathol. 211*, 134–143. (b) Kroemer, G., and Jaattela, M. (2005) Lysosomes and autophagy in cell death control. *Nat. Rev. Cancer 5*, 886–897.
43. Arbeloa, F. L., Banuelos, J., Martinez, V., Arbeloa, T., and Arbeloa, I. P. (2005) Structural, photophysical and lasing properties of pyrromethene dyes. *Int. Rev. Phys. Chem. 24*, 339–374.
44. We note, however, that under our experimental conditions, we work well above the DMPC transition temperature.
45. Alessi, M., Paul, T., Scaiano, J. C., and Ingold, K. U. (2002) The Contrasting Kinetics of Peroxidation of Vitamin E-Containing Phospholipid Unilamellar Vesicles and Human Low-Density Lipoprotein. *J. Am. Chem. Soc. 124*, 6957–6965.
46. Atkinson, J., Epand, R. F., and Epand, R. M. (2008) Tocopherols and tocotrienols in membranes: A critical review. *Free Radical Biol. Med. 44*, 739–764.
47. Wang, X., and Quinn, P. J. (1999) Vitamin E and its function in membranes. *Prog. Lipid Res. 38*, 309–336.
48. (a) Wang, X., and Quinn, P. J. (2000) The location and function of vitamin E in membranes. *Mol. Membr. Biol. 17*, 143–156. (b) Quinn, P. J. (2007) *Vitamin E: Vitamins and Hormones Advances in Research and Applications* , Vol. *76*, p 67, Elsevier, Amsterdam.
49. Fukuzawa, K., Ikebata, W., Shibata, A., Kumadaki, I., Sakanaka, T., and Urano, S. (1992) Location and dynamics of α-tocopherol in model phospholipid membranes with different charges. *Chem. Phys. Lipids 63*, 69–75.
50. Maggio, B., Diplock, A. T., and Lucy, J. A. (1977) Interactions of tocopherols and ubiquinones with monolayers of phospholipids. *Biochem. J. 161*, 111–121.
51. Korlach, J., Schwille, P., Webb, W. W., and Feigenson, G. W. (1999) Characterization of lipid bilayer phases by confocal microscopy and fluorescence correlation spectroscopy. *Proc. Natl. Acad. Sci. U.S.A. 96*, 8461–8466.
52. Lopez, E., Arce, C., Oset-Gasque, M. J., Canadas, S., and Gonzalez, M. P. (2006) Cadmium induces reactive oxygen species generation and lipid peroxidation in cortical neurons in culture. *Free Radical Biol. Med. 40*, 940–951.
53. Cho, S. J., Maysinger, D., Jain, M., Roder, B., Hackbarth, S., and Winnik, F. M. (2007) Long-term exposure to CdTe quantum dots causes functional impairments in live cells. *Langmuir 23*, 1974–1980.
54. Buttriss, J. L., and Diplock, A. T. (1988) The ga-tocopherol and phospholipid fatty acid content of rat liver subcellular membranes in vitamin E and selenium deficiency. *Biochim. Biophys. Acta 963*, 61–69.
55. Czibener, C., Sherer, N. M., Becker, S. M., Pypaert, M., Hui, E., Chapman, E. R., Mothes, W., and Andrews, N. W. (2006) Ca^{2+} and synaptotagmin VII-dependent delivery of lysosomal membrane to nascent phagosomes. *J. Cell Biol. 174*, 997–1007.
56. Moreira, P. I., Harris, P. L., Zhu, X., Santos, M. S., Oliveira, C. R., Smith, M. A., and Perry, G. (2007) Lipoic acid and N-acetyl cysteine decrease mitochondrial-related oxidative stress in Alzheimer disease patient fibroblasts. *J. Alzheimer's Dis. 12*, 195–206.